Use of Variable Threshold Detection in Time of Arrival Measurements for SBL Underwater Acoustic Positioning Systems

SHINGO YOSHIZAWA
Faculty of Engineering,
Kitami Institute of Technology,
Koen-Cho 165, Kitami, 090-8507,
JAPAN

Abstract: - Underwater acoustic positioning systems (UAPSs) are used to know the positions of underwater vehicles and sensors. In short baseline (SBL) acoustic positioning systems, the three-dimensional position is localized by the measured distances, where the distance is obtained by estimating the time of arrivals (TOAs). In underwater acoustics, the TOA measurement errors are caused by acoustic reflection and ambient noise. The typical TOA measurement is done by detecting the time location of the maximum correlation peak. This peak detection causes a measurement error when the first peak is not the maximum amplitude. We propose the variable threshold detection to keep high positioning accuracy in highly reflective and noisy environments. The results of our simulation and experiment have proved the effectiveness of the proposed method.

Key-Words: - Underwater acoustic positioning systems, short baseline, time of arrival, multipath interference, acoustic reflection, variable threshold.

Received: May 14, 2024. Revised: October 17, 2024. Accepted: November 13, 2024. Published: December 27, 2024.

1 Introduction

Underwater acoustic positioning systems (UAPSs) play an important role in knowing the positions of underwater vehicles such as remotely operated vehicles (ROVs) and autonomous underwater vehicles (AUVs), [1], [2]. In addition, the UAPS is essential for sensor nodes to be aware of their positions in underwater acoustic sensor networks, [3], [4]. The operation methods of UAPS are generally categorized into three types, called as long baseline (LBL), short baseline (SBL), and ultra-short baseline (USBL), [5]. In LBL and SBL, the three-dimensional position is localized by the measured distance, where the distance is obtained by estimating the time of arrivals (TOAs). USBL estimates the time difference of arrivals (TDOAs) with a small array of receiver elements.

In USBL, we tackled the improvement of TDOA measurement under highly reflective and noisy environments. A TDOA is computed from an arrival time difference between received signals by a correlation function, where generalized cross-correlation with phase transform (GCC-PHAT) [6] and matched filter (MF) [7] are typically used. However, the TDOA measurement is strongly influenced by the reflection of sound waves. In underwater acoustics, many reflected waves are caused by the reflection on the water surface, bottom, and obstacles. This phenomenon is known as multipath interference, which generates the pseudo-peaks in the correlation function.

In our previous work, we presented impulse response-based GCC-PHAT (IR-GCC-PHAT) to cope with multipath interference, [8]. IR-GCC-PHAT computes a time difference by taking a cross-correlation between two impulse responses. We demonstrated that IR-GCC-PHAT shows higher position accuracy than GCC-PHAT and MF in the evaluation of simulation and experiment.

The appropriate receiver element spacing in USBL is less than several tens of centimeters. When the element spacing is more than one meter in SBL, we should consider the DOA estimation errors when the sound waves arriving at the two receiver elements cannot be assumed to be plane waves. In SBL, the target of a sound source is localized by multiple distances.

This paper focuses on improving the TOA measurement algorithm. In typical TOA measurements, the cross-correlation function between received and reference signals is computed and a TOA is detected by the maximum correlation peak, [9]. This method sometimes induces estimation errors in a highly reflective environment, where some of the multipath signals are received stronger than the line-of-sight (LoS) signal. The fixed threshold detection is effective for highly reflective environments [10], where the first peak correlation is at least 50% of the maximum correlation is detected.

The fixed threshold detection is robust with acoustic reflections, however the detection performance decreases under noisy environments. In this paper, we propose a new method of using variable threshold detection that the peak detection is stable in both reflective and noisy environments. The key idea is to use the TDOA measurement algorithm such as IR-GCC-PHAT to check whether a threshold is appropriate.

In this paper, we set a goal to locate two-dimensional coordinates by the TOA measurement. When the positioning target is an underwater robot, an accurate *z*-coordinate position is available by employing a depth sensor. For example, we demonstrated that the use of a single TDOA and depth information provides higher positioning accuracy than multiple TDOAs in USBL, where we evaluated positioning accuracy by the condition of one source and two receiver elements.

This paper is organized as follows. Section 2 introduces the methods for calculating positioning coordinates and compares positioning accuracy between TDOA and TOA measurements in UBSL. Section 3 explains the conventional detection methods in the TOA measurement. Section 4 presents the proposed detection method. Section 5 reports the experimental results in acoustic positioning. Section 6 discusses the proposed and conventional methods given the simulation results. Section 7 summarizes our work.

2 Calculation Methods of Positioning Coordinates

2.1 Two-dimensional Localization

We assume that the two-dimensional coordinates are calculated assuming that the height positions of the sound source and the receiver elements are the same. When the height position of the sound source is known, as measured by the depth sensor, the conversion from two-dimensional to three-dimensional coordinates is straightforward.

There are two methods to calculate the positioning position of a target using two receiver elements. The first method calculates with one angle of arrival and one distance, and the second method calculates with two distances.

The two methods of calculating positioning coordinates are illustrated in Figure 1. Note that the angle of arrival and the distance are estimated by TDOA and TOA measurements, respectively. When the coordinates of the sound source and receiver elements are represented by $(x_{\mathrm{t}}, y_{\mathrm{t}}), (x_{\mathrm{r1}}, y_{\mathrm{r1}})$ and $(x_{\mathrm{r2}}, y_{\mathrm{r2}})$, the coordinates of source in Figure 1(a) are calculated as:

$$\acute{x}_t = x_{\mathrm{r1}} + D\cos\theta \tag{1}$$

$$\acute{y}_t = y_{\mathrm{r1}} + D\sin\theta \tag{2}$$

$$\theta = \arcsin\left(\frac{c\tau}{R}\right), \tag{3}$$

where θ is the angle of arrival and D is the distance between the sound source and the first receiver element. The underwater sound speed and receiver element space are expressed by c [m/s] and R [m].

As for the localization by the measurement of TOAs in Figure 1(b), the coordinates of source are calculated as:

$$\acute{x}_t = x_{\mathrm{r1}} + \frac{D_1^2 - D_2^2 + R^2}{2R} \tag{4}$$

$$\acute{y}_t = y_{\mathrm{r1}} + \sqrt{D_1^2 - \acute{x}_t^{\,2}}\ , \tag{5}$$

where D_1 and D_2 are the distances between the sound source and the first and second receiver elements.

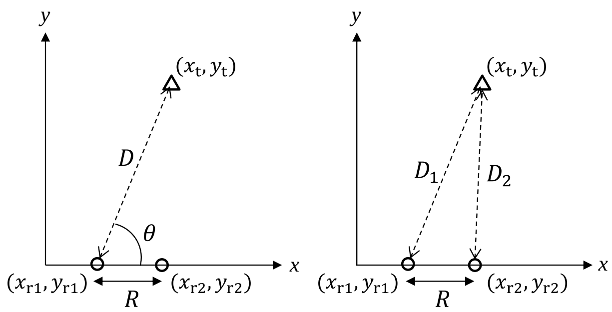

(a) Measurement of a TDOA (b) Measurement of TOAs

Fig. 1: Methods of calculating positioning coordinates

2.2 TDOA Measurement

Although most of the explanations in TDOA algorithms have been made in [8], we describe some of them again for readability.

Two received signals $y_1(k)$ and $y_2(k)$ can be modeled by using a transmitted signal $x(k)$ and impulse responses $h_1(k)$ and $h_2(k)$ that express a propagation path from a transmitter to a receiver as

$$y_1(k) = h_1(k) * x(k) + n_1(k) \tag{6}$$

$$y_2(k) = h_2(k) * x(k) + n_2(k), \tag{7}$$

where k indicates a discrete time index and $*$ shows a convolution operation. $n_1(k)$ and $n_2(k)$ are noise components uncorrelated with the transmitted signal. The received signals can be expressed in frequency domain as:

$$Y_1(l) = \mathrm{DFT}_N[y_1(k)] = H_1(l)X(l) + N_1(l) \quad (8)$$

$$Y_2(l) = \mathrm{DFT}_N[y_2(k)] = H_2(l)X(l) + N_2(l). \quad (9)$$

$\mathrm{DFT}_N[\cdot]$ indicates the discrete Fourier transform for N samples and l denotes a discrete frequency index.

GCC-PHAT algorithm [6] is given by the following equation:

$$\Phi_{\mathrm{GCC-PHAT}}(k) = \mathrm{IDFT}_N\left[\frac{Y_1(l)Y_2^*(l)}{|Y_1(l)Y_2^*(l)|}\right]. \quad (10)$$

The time difference is detected by the highest peak detection as:

$$\tau_{\mathrm{GCC-PHAT}} = \underset{k}{\mathrm{argmax}}\, \Phi_{\mathrm{GCC-PHAT}}(k), \quad (11)$$

The estimated time difference is converted into the angle of arrival as explained in (3).

IR-GCC-PHAT algorithm is the improved version of GCC-PHAT [8]. In UAPS, an artificially generated signal such as a pseudo-noise (PN) code sequence can be utilized as a sound source. It indicates that $x(k)$ ($X(l)$ in frequency domain) can be treated as a known parameter. IR-GCC-PHAT directly computes the two impulse responses by the frequency-domain division that is expressed as

$$h_1'(k) = \mathrm{IDFT}_N[Y_1(l)/X(l)] \quad (12)$$

$$h_2'(k) = \mathrm{IDFT}_N[Y_2(l)/X(l)]. \quad (13)$$

The time difference can be detected by the cross-correlation function after taking absolute values for the two impulse responses:

$$G_1(l) = \mathrm{DFT}_N[|h_1'(k)|] \quad (14)$$

$$G_2(l) = \mathrm{DFT}_N[|h_2'(k)|] \quad (15)$$

$$\Phi_{\mathrm{IR}}(k) = \mathrm{IDFT}_N\left[\frac{G_1(l)G_2^*(l)}{|G_1(l)G_2^*(l)|}\right] \quad (16)$$

$$\tau_{\mathrm{IR}} = \underset{k}{\mathrm{argmax}}\, \Phi_{\mathrm{IR}}(k). \quad (17)$$

IR-GCC-PHAT is robust with noisy and reverberant environments and provides higher positioning accuracy than GCC-PHAT and MF.

2.3 TOA Measurement

There are two methods of distance measurement in UAPS. One is to measure a round trip time (RTT) by an acoustic transponder. The other is to measure one-way propagation time assuming that a sound source and a receiver have the same clock time. For example, time synchronization has been achieved by integrating a chip-scale atomic clock (CSAC) into an acoustic modem [11]. The latter is addressed in this paper.

When the signal start times are identical among the sound source and receivers, we can take the two cross-correlations as:

$$\Phi_1(k) = \mathrm{IDFT}_N[Y_1(l)X^*(l)] \quad (18)$$

$$\Phi_2(k) = \mathrm{IDFT}_N[Y_2(l)X^*(l)] \quad (19)$$

$$T_1 = \underset{k}{\mathrm{argmax}}\, |\Phi_1(k)| \quad (20)$$

$$T_2 = \underset{k}{\mathrm{argmax}}\, |\Phi_2(k)|. \quad (21)$$

The TOAs are converted into the distances by

$$D_1 = cT_1 \quad (22)$$

$$D_2 = cT_2. \quad (23)$$

In (20) and (21), each TOA can be detected by the maximum correlation peak. We call it the maximum value detection. The maximum value detection is sensitive to acoustic reflections, which is to be explained in Section 3.

2.4 Positioning Accuracy in TDOA and TOA Measurements

The TDOA measurement is mainly used for USBL, where the receiver spacing is less than several tens of centimeters. It assumes that the sound source is located farther from the receiver and that the plane wave reaches the receiver elements.

The positioning accuracy in the TDOA and TOA measurements are compared by our simulation, where the simulation results are shown in Figure 2. This simulation condition is close to being ideal, where a signal-to-noise ratio (SNR) of 30 dB with non-acoustic reflection is set. Please see the other conditions such as sound source and receiver locations in Section 5. The positioning coordinates in the TDOA and TOA measurements are computed by (1), (2), (4), and (5).

The positioning results for the small array spacing (R=0.1) are plotted in Figure 2(a). The averages of positioning errors are 0.58 m and 0.34 m for the TDOA and TOA measurements. The positioning accuracy of the two measurements is approximately the same.

The positioning results for the large array spacing (R=1) are plotted in Figure 2(b). The averages of positioning errors are 0.37 m and 0.04 m for the TDOA and TOA measurements. The TOA measurement can improve positioning accuracy, whereas the TDOA measurement does not. The angle estimation in (3) assumes that a plane wave reaches the two receiver elements. This assumption is no longer valid for the large spacing. When the receiver spacing is more than one meter, the TDOA measurement cannot provide high positioning accuracy anymore.

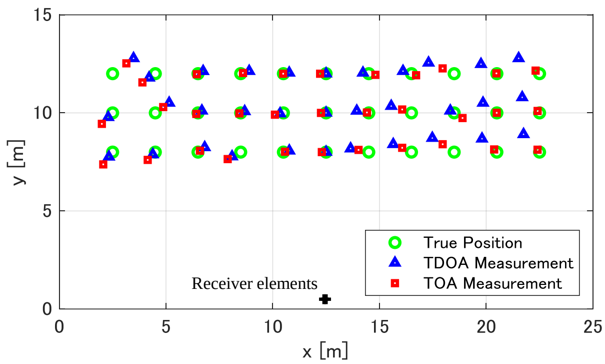

(a) Positioning results for array spacing of 0.1 m

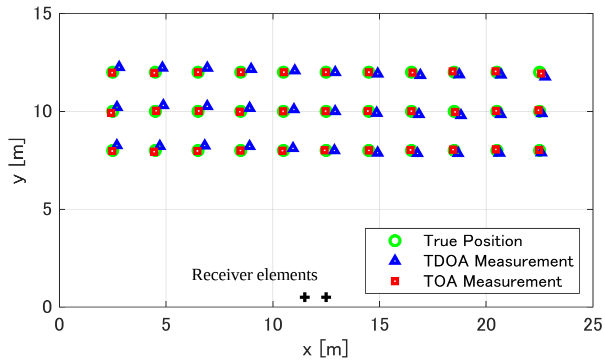

(b) Positioning results for array spacing of 1 m

Fig. 2: Comparison of TDOA and TOA measurements

3 Conventional Methods

3.1 Maximum Value Detection

The maximum value detection is widely used for the TOA measurement. Each TOA is detected at the point of having the highest value in the cross-correlation, [9]. The maximum value detection has the disadvantage of being sensitive to acoustic reflections.

Figure 3 shows an example where the maximum value detection induces a measurement error under a reflective environment. Note that the cross-correlation functions of $|\Phi_1(k)|$ and $|\Phi_2(k)|$ are normalized so that the value of maximum peak becomes 1. As shown in Figure 3(a), the correct TOAs can be detected under the non-reflective environment.

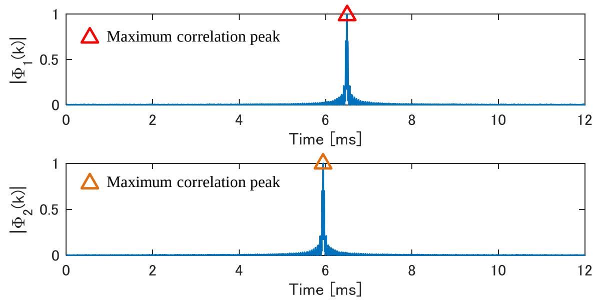

(a) Non-reflective environment

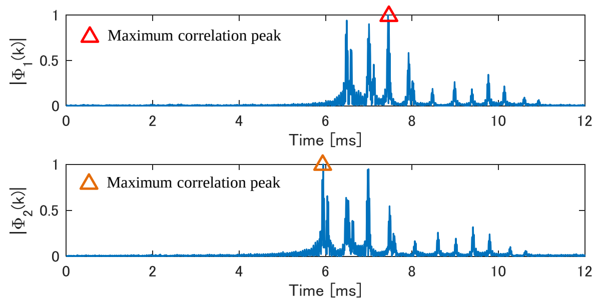

(b) Reflective environment

Fig. 3: Influence of acoustic reflection in maximum value detection

Multiple correlation peaks are observed in Figure 3(b). These peaks are caused by acoustic reflections, where the sound wave reflects on water surface, bottom, and surrounding walls. When we look at the graph of $|\Phi_1(k)|$, the maximum value detection cannot find the point of the first peak, which outputs an incorrect TOA.

The situation that the first peak does not have the highest value can be explained by the relationship between propagation path and impulse response as illustrated in Figure 4.

When a sound wave reaches the receiver following a direct or reflected path, its arrival time and reception intensity are expressed as an impulse response. The impulse response can be observed by measuring the cross-correlation functions as examples in Figure 3. When the path lengths of the two paths are identical, the signals are combined on the same arrival time. The magnitude of the synthesized reflected path surpasses that of the direct path.

Another factor is the directivity of the receiver hydrophone. The directivity of the receiver is not completely omnidirectional, even if it is noted in the specifications. Due to the sensitivity variations depending on the location on the surface of the hydrophone, the received intensity for the direct path may be small.

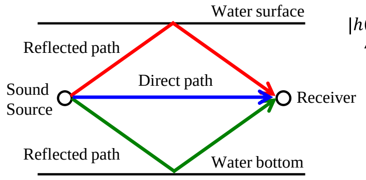

(a) Propagation path

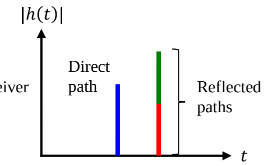

(b) Impulse response

Fig. 4: Relationship between propagation path and impulse response

3.2 Fixed Threshold Detection

The fixed threshold detection can find the first peak even if the first peak does not have the maximum magnitude, [10]. The procedure of threshold detection is illustrated in Figure 5, where a threshold is set to 0.5 for the maximum value of 1 in the cross-correlation functions.

Figure 5(a) shows how the threshold detection can get correct TOAs even in a reflective environment. The detected points correspond to the propagation time in the direct path.

Although the fixed threshold detection is effective for reflective environments, the detection degrades under noisy environments. Many pseudo peaks appear on the correlation function under the low SNR condition of Figure 5(b). Since the magnitude of their pseudo peaks surpasses 0.5, the threshold detection cannot find the true peak derived from the direct path.

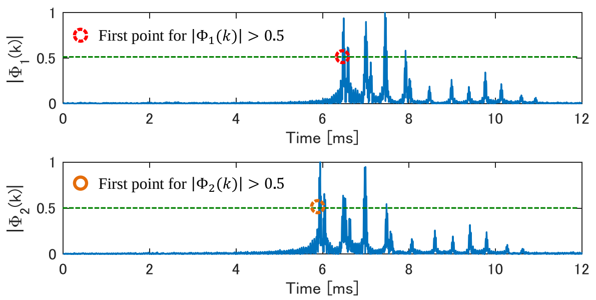

(a) Reflective environment with a SNR of 30 dB

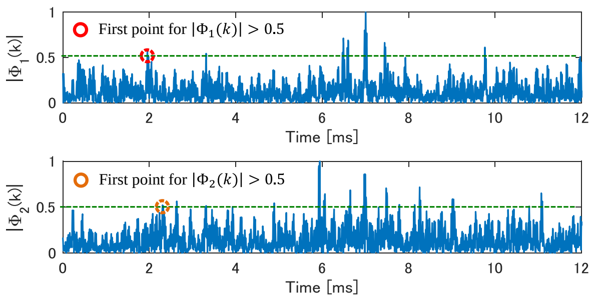

(b) Reflective environment with a SNR of −7 dB

Fig. 5: Influence of acoustic reflection and noise in fixed threshold detection

4 Proposed Method

We apply the variable threshold that a threshold can be changed according to surrounding environments. Since the magnitude of the first peak is unknown, the threshold should be as small as possible. However, a small threshold tends to have false detection due to the pseudo-peaks derived from background noise.

The key idea is to check whether a threshold is appropriate in some way. We employ the TDOA measurement using IR-GCC-PHAT for checking a threshold, where the cross-correlation functions of $|\Phi_{IR}(k)|$ are shown in Figure 6. The arrival time difference is detected according to (17). Unlike the results of Figure 3 and Figure 5, the expected time differences detected are similar. IR-GCC-PHAT is robust with both reflective and noisy environments [8].

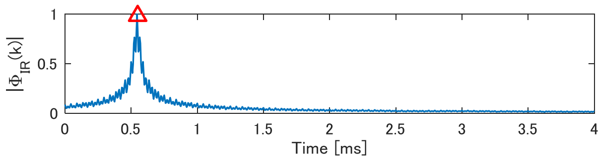

(a) Non-reflective environment with a SNR of 30 dB

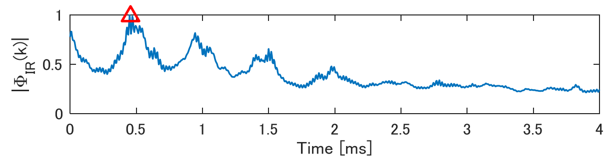

(b) Reflective environment with a SNR of 30 dB

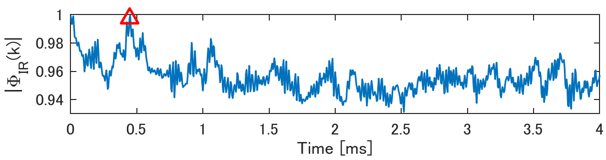

(c) Reflective environment with a SNR of −7 dB

Fig. 6: Cross-correlation functions in TDOA measurement

Although the TDOA measurement with a small receiver array does not provide an accurate arrival time difference (see Section 2.4), it is suitable for only verifying that the threshold is appropriate. We compare the arrival time differences estimated by the TDOA and TOA measurements as:

$$\theta_{TDOA} = \arcsin\left(\frac{c\tau_{IR}}{R}\right) \quad (24)$$

$$\theta_{TOA} = \arcsin\left(\frac{c(T_1 - T_2)}{R}\right) \quad (25)$$

$$\Delta\theta = |\theta_{TDOA} - \theta_{TOA}|. \quad (26)$$

If $\Delta\theta$ is within a certain range, the time difference obtained from the TOA measurement is reasonable and the threshold is also appropriate.

The flowchart of the proposed method is shown in Figure 7, where the variable threshold is given by ξ. The initial threshold is set to 0.3 and increased by each iteration loop processing. The two TOAs are finalized when the conditions of $\Delta\theta < 10$ deg. or $\xi \geq 0.9$ are satisfied. The small threshold can detect the first peak in a reflective environment and the large threshold cope with a noisy environment.

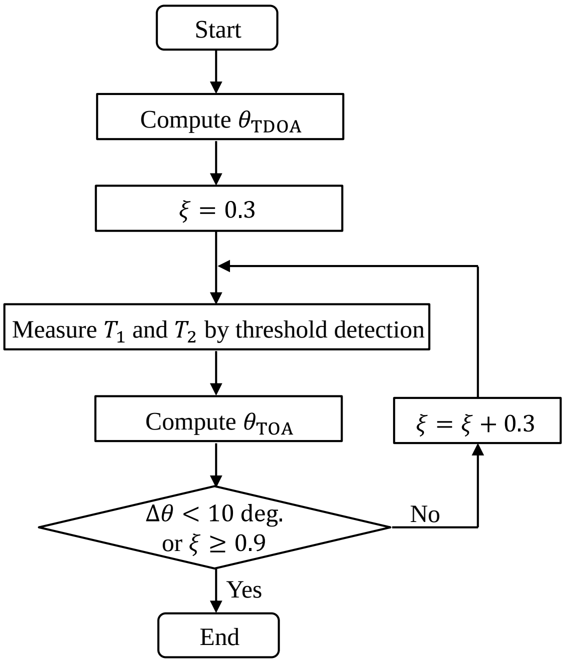

Fig.7: Flowchart of variable threshold detection

5 Evaluation

5.1 Experimental Conditions

Our underwater acoustic positioning experiment was conducted in the swimming pool. The experimental scenery is shown in Figure 8.

Table 1 presents the specifications of the transmitted signal and the experimental conditions. We generate the transmit signal (corresponding to a sound source) by using PN code sequences. The frequency band of the transmitted signal is 12 kHz to 32 kHz, and it is a flat spectrum with approximately $|X(l)| = 1$ within the band. The acoustic field size is 25 × 15 × 1.35 m for length, width, and height.

The locations of the transmitter (TX) and receiver elements (RX1 and RX2) are shown in Figure 9. TX is moved every 2 m along the x-axis (2.5 to 22.5 m) and the y-axis (8 to 12 m). RX1 is fixed at x=12.5 m and y=0.5 m with an interval of 1.4 m between the receiver elements. The height of the transmitter and receiver elements is set to the same 0.8 m.

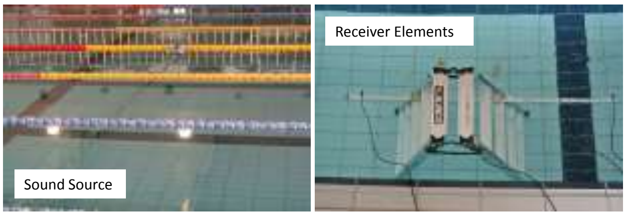

Fig. 8: Experimental scenery

Table 1. Specifications of transmitted signal and simulation conditions

Sampling frequency	200 kHz
Frequency band	12 kHz - 32 kHz
Transmitted signal	Pseudo-noise (PN) sequence
Signal length	81.9 ms
Number of signal points	16,384
Number of receivers	2
Receiver array spacing	1.4 m
Acoustic field	25 × 15 × 1.35 m

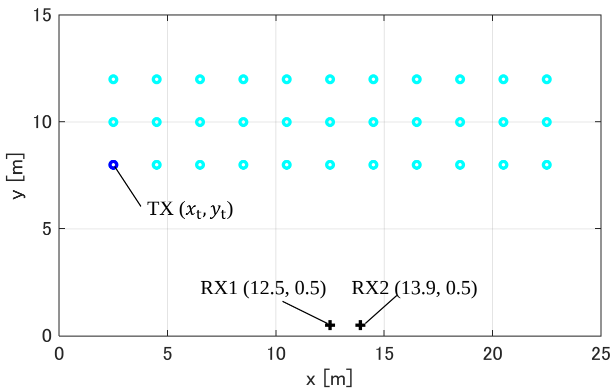

Fig. 9: Locations of transmitter and receiver elements

We compare positioning accuracy in the two conventional methods and the proposed method, i.e., the maximum value detection, the fixed threshold detection, and the variable threshold detection. Three measurements are taken per TX location and the two-dimensional coordinates are calculated according to (4) and (5). We adjust the amplitude of noise signals and add them to the received signals to evaluate various SNR conditions.

5.2 Experimental Results

The experimental results in a high SNR condition are shown in Figure 10. The maximum value detection tends to have large positioning errors when the sound source is near the wall. The sound waves reflected from the side walls interfere strongly in the swimming pool. The error average of maximum value detection is larger than those of the fixed threshold detection the variable threshold detection.

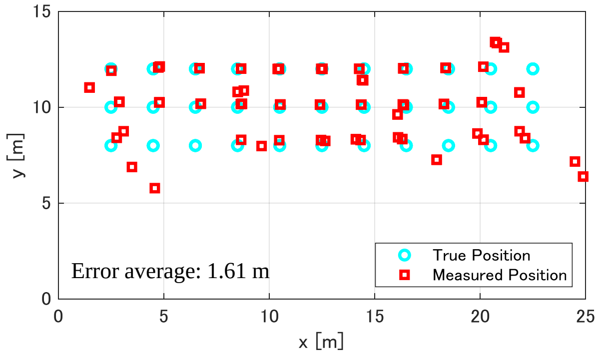

(a) Maximum value detection with a SNR of 5 dB

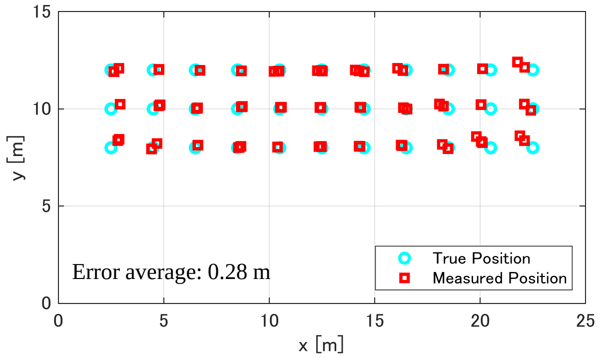

(b) Fixed threshold detection with a SNR of 5 dB

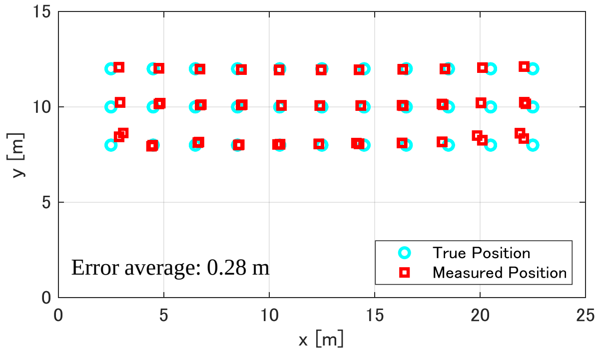

(c) Variable threshold detection with a SNR of 5 dB

Fig. 10: Experimental results in a high SNR condition

The error averages between the fixed threshold detection and the variable threshold detection are similar. It indicates that a threshold of around 0.5 is appropriate in this SNR condition.

The experimental results in a low SNR condition are shown in Figure 11. While the variable threshold detection keeps high positioning accuracy, the fixed threshold detection increases the error average. Since the fixed threshold was set to 0.5, some TOA measurements failed due to the pseudo peaks derived from background noise.

Table 2 summarizes the experimental results for all SNR conditions. The maximum value detection shows larger positioning errors for the SNR conditions of 5 dB and 0 dB.

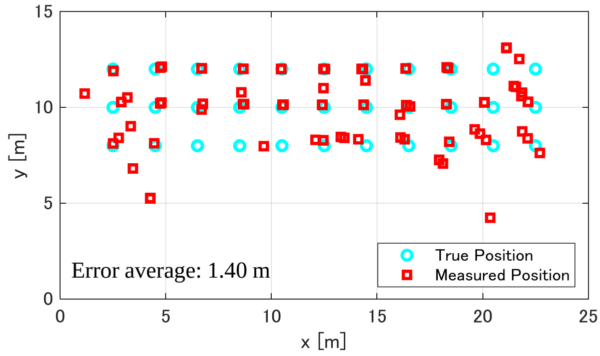

(a) Maximum value detection with a SNR of −5 dB

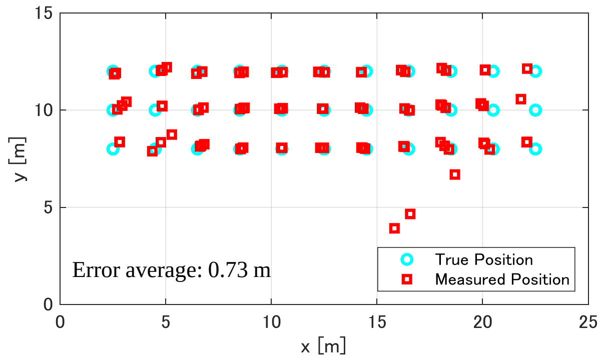

(b) Fixed threshold detection with a SNR of −5 dB

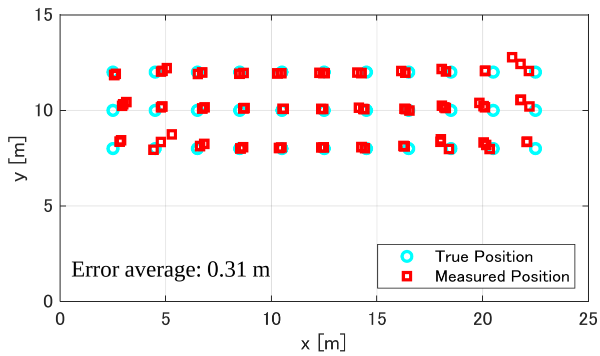

(c) Variable threshold detection with a SNR of −5 dB

Fig. 11: Experimental results in a low SNR condition

The fixed threshold detection degrades positioning accuracy for the SNR conditions of −5 dB and 0 dB. The variable threshold detection can keep the highest positioning accuracy even for all SNR conditions.

Table 2. Average positioning errors [m] for all SNR conditions

SNR [dB]	Maximum value detection	Fixed threshold detection	Variable threshold detection
5	1.61	0.28	0.28
0	1.65	0.28	0.28
−5	1.40	0.73	0.31
−10	1.87	6.97	1.16

6 Discussion

We evaluate positioning accuracy for various conditions in simulation. We use a sound wave propagation simulator that tracks sound waves by the mirror image method. The sound wave propagation simulator reproduces acoustic reflections where a user specifies the size of acoustic field space, reflectance ratios on six boundaries, and sound source and receiver positions. The locations of the sound source and receiver elements and the signal specifications are the same as those in the experiment.

Table 3 shows the results of average positioning errors under a non-reflective environment, where all reflectance ratios are set to 0. Since only the peak in derived from the direct path appears in the correlation function as shown in Figure 3(a), the maximum value detection gives the highest positioning performance for the low SNR conditions of less than −10 dB.

While the variable threshold detection slightly decreases positioning accuracy at the SNR of −10 dB, the fixed threshold detection significantly degraded its performance. The threshold of 0.5 would be insufficient in this SNR condition.

Table 4 shows the results of average positioning errors under a reflective environment. The reflectance ratios are set to 1 for the water surface and 0.7 for the water bottom and the surrounding walls. The maximum value detection shows large positioning errors due to acoustic reflections. The variable threshold detection shows better performance than the fixed threshold detection for the low SNR conditions of less than −5 dB.

We confirmed that the variable threshold detection can cope with noisy and reflective environments.

Table 3. Simulation results under a non-reflective environment

SNR [dB]	Maximum value detection	Fixed threshold detection	Variable threshold detection
5	0.02	0.02	0.02
0	0.02	0.02	0.02
−5	0.02	0.02	0.02
−10	0.02	3.36	0.08
−15	22.87	10.74	6.12

Table 4. Simulation results under a reflective environment

SNR [dB]	Maximum value detection	Fixed threshold detection	Variable threshold detection
5	2.48	0.02	0.02
0	3.91	0.04	0.03
−5	4.62	9.62	1.94
−10	26.83	10.86	10.26

7 Conclusion

This paper has presented a method of variable threshold detection for SBL underwater acoustic positioning systems. We explained the three methods in the TOA measurement. The maximum value detection and the fixed threshold detection suffer from noise interference and acoustic reflections. The variable threshold detection can find an appropriate threshold by using the estimated angle in the TDOA measurement. The experimental and simulation results have proved that the proposed method outperforms the conventional methods in positioning accuracy.

Our future work will focus on the improvement of positioning accuracy when a source target is moving at high speed. The countermeasure of Doppler shifts will be discussed.

Acknowledgement:
The authors would like to thank Mr. Shuhei Habu for his support and assistance with this research.

Declaration of Generative AI and AI-assisted Technologies in the Writing Process

During the preparation of this work the author used Grammarly and DeepL services in order to correct and improve the quality of English writing. After using this tool/service, the author reviewed and edited the content as needed and takes full responsibility for the content of the publication.

References:

[1] L. Paull, S. Saeedi, M. Seto and H. Li, "AUV navigation and localization: a review," *IEEE Journal of Oceanic Engineering*, vol. 39, no. 1, pp. 131-149, Jan. 2014, doi: 10.1109/JOE.2013.2278891.

[2] D. Thomson and S. Dosso, "AUV localization in an underwater acoustic positioning system," *MTS/IEEE OCEANS-Bergen*, Bergen, Norway, pp. 1-6, June 2013, doi: 10.1109/OCEANS-Bergen.2013.6608140.

[3] I. Ullah, J. Chen, X. Su, C. Esposito and C. Choi, "Localization and detection of targets in underwater wireless sensor using distance and angle based algorithms," *IEEE Access*, vol. 7, pp. 45693-45704, Apr. 2019, doi: 10.1109/ACCESS.2019.2909133.

[4] J. Luo, Y. Yang, Z. Wang and Y. Chen, "Localization algorithm for underwater sensor network: a review," *IEEE Internet of Things Journal*, vol. 8, no. 17, pp. 13126-13144, Sep. 2021, doi: 10.1109/JIOT.2021.3081918.

[5] Otero P, Hernández-Romero Á, Luque-Nieto M-Á, Ariza A, "Underwater positioning system based on drifting buoys and acoustic modems," *Journal of Marine Science and Engineering*, vol. 11, no. 4, pp.1-9, Mar 2023, doi: 10.3390/jmse11040682.

[6] J. Choi, J. Park, Y. Lee, J. Jung, and H. Choi, "Robust directional angle estimation of underwater acoustic source using a marine vehicle," *MDPI Sensors*, vol. 18, issue 9, pp. 1-14, Sep. 2018, doi: 10.3390/s18093062.

[7] B. Kouzoundjian, F. Beaubois, S. Reboul, and J. B. Choquel, and J. Noyer, "A TDOA underwater localization approach for shallow water environment," *MTS/IEEE OCEANS-Aberdeen*, Aberdeen, UK, pp. 1-4, June 2017, doi: 10.1109/OCEANSE.2017.8085030.

[8] S. Yoshizawa, "Underwater acoustic localization based on IR-GCC-PHAT in reverberant environments," *International Journal of Circuits, Systems and Signal Processing*, Vol. 15, pp.164-171, Mar. 2021, doi:10.46300/9106.2021.15.18.

[9] Y. Wu, Y. Liu, S. Yan and L. Yang, "The improvement of acoustic positioning of underwater vehicles based on synthetic long baseline navigation," *MTS/IEEE OCEANS 2017-Aberdeen*, Aberdeen, UK, pp. 1-5, June 2017, doi: 10.1109/OCEANSE.2017.8084593.

[10] W. A. P. van Kleunen, K. C. H. Blom, N. Meratnia, A. B. J. Kokkeler, P. J. M. Havinga and G. J. M. Smit, "Underwater localization by combining time-of-flight and direction-of-arrival," *MTS/IEEE OCEANS 2014-Taipei*, Taipei, Taiwan, pp.1-6, Apr. 2014, doi: 10.1109/OCEANS-TAIPEI.2014.6964309.

[11] M. V. Jakuba, J. W. Partan, S. E. Webster, D. Giaya and C. Ramirez, "Performance of a low-power one-way travel-time inverted ultra-short baseline navigation system," *MTS/IEEE OCEANS 2021-San Diego*, San Diego, CA, USA, pp. 1-10, Sep, 2021 doi: 10.23919/OCEANS44145.2021.9705795.

Contribution of Individual Authors to the Creation of a Scientific Article (Ghostwriting Policy)

The authors equally contributed in the present research, at all stages from the formulation of the problem to the final findings and solution.

Sources of Funding for Research Presented in a Scientific Article or Scientific Article Itself

No funding was received for conducting this study.

Conflict of Interest

The authors have no conflicts of interest to declare.